Nuclear Physics A549 (1992) 439–460
North-Holland

NUCLEAR
PHYSICS A

Model calculations of doubly closed shell nuclei in CBF theory (I)

G. Co'
INFN, Sezione di Lecce, I-73100 Lecce, Italy

A. Fabrocini
Department of Physics, University of Pisa and INFN, Sezione di Pisa, I-56100 Pisa, Italy

S. Fantoni
Interdisciplinary Laboratory for Advanced Studies (ILAS) and INFN, Sezione di Trieste, I-34014 Trieste, Italy

I.E. Lagaris
Department of Physics, University of Ioannina, Ioannina, Greece

Received 8 May 1992

Abstract: Correlated basis function theory and Fermi hypernetted chain theory are extended to treat finite Fermi systems. In this first paper, the effects of the scalar nucleon–nucleon correlations are investigated by studying some model $N = Z$ nuclei. Results of calculations performed using central nucleon–nucleon potentials, without tensor components, are presented and are compared with results from other theories.

1. Introduction

In recent years much progress has been made in the development of the non-relativistic nuclear many-body theory aiming to describe the properties of all the nuclear systems, from deuterons to nuclear matter, by means of the hamiltonian

$$H = -\frac{\hbar^2}{2m}\sum_i \nabla_i^2 + \sum_{i<j} v_{ij} + \sum_{i<j<k} V_{ijk}, \tag{1.1}$$

where the two-body potential v_{ij} is required to fit the deuteron and the nucleon–nucleon scattering data, and the three-body potential V_{ijk} is needed to have a good description of both light nuclei and nuclear-matter properties.

The two- and three-nucleon potentials, v_{ij} and V_{ijk}, are unambiguously determined at large interparticle distances by meson exchange processes. At intermediate and short distances semi-microscopic or purely phenomenological descriptions are usually adopted. Several realistic potentials, satisfying the above requirements, are

Correspondence to: Dr. A. Fabrocini, Department of Physics, Piazza Torricelli 2, I-56100 Pisa, Italy.

now widely used in modern nuclear many-body theories and all lead to comparable results [1]).

Light nuclei have been successfully described within different approaches. Faddeev [2]) and Green function Monte Carlo (GFMC) [3]) theories solve exactly the many-body Schrödinger equation in the $A = 3, 4$ cases for several nuclear potentials.

Variational methods [4,5]), are also very successful in describing the ground-state properties of light nuclei and moreover, they allow for accurate studies of the dynamical properties of these systems.

For heavier systems, no exact method has been so far able to deal with realistic interactions. GFMC has been used in ^{16}O but only with a simplified interaction [6]).

Microscopic calculations, based on the hamiltonian (1.1), have been performed for studying the equation of state of the infinite systems of nucleons, such as neutron and nuclear matter, by using standard perturbation theory [7]) or correlated basis function (CBF) theory [8,9]).

The development of the CBF theory in the last decade, has allowed for microscopic and reliable evaluations of the dynamical properties, such as momentum distribution and electromagnetic responses, of both light nuclei and nuclear matter [4,9]).

The CBF theory is based on a set of correlated A-body wave functions,

$$\Psi_n(1, 2, \ldots, A) = F(1, 2, \ldots, A)\Phi_n(1, 2, \ldots, A), \tag{1.2}$$

where $\Phi_n(1, 2, \ldots, A)$ is the generic mean-field state (a Slater determinant of plane waves in nuclear matter), $F(1, 2, \ldots, A)$ is an A-body correlation operator acting on Φ_n. A correlation operator, which has been found to properly take into account the correlations induced by the nuclear hamiltonian, has the following form:

$$F(1, \ldots, A) = \prod_{i<j} f(r_{ij}) \mathcal{S}\left(\prod_{i<j} f_{\mathrm{SD}}(i, j) \right). \tag{1.3}$$

In the above equation $f(r_{ij})$ is a scalar two-body correlation function depending on the interparticle distance r_{ij} only (Jastrow factor) and $\mathcal{S}$ is the symmetrizer of the product of the state-dependent correlation factors $f_{\mathrm{SD}}(i, j)$ given by

$$f(r_{ij}) f_{\mathrm{SD}}(i, j) = 1 + \sum_{n=1} \mathcal{F}^{(n)}(r_{ij}) O^{(n)}(i, j). \tag{1.4}$$

We have for the scalar component $\mathcal{F}^{(n=1)}(r_{ij}) = f(r_{ij}) - 1$. The operators $O^{(n)}(i, j)$ include the central components ($n = 1, 4$), $(1, \boldsymbol{\sigma}_i \cdot \boldsymbol{\sigma}_j, \boldsymbol{\tau}_i \cdot \boldsymbol{\tau}_j, \boldsymbol{\sigma}_i \cdot \boldsymbol{\sigma}_j \boldsymbol{\tau}_i \cdot \boldsymbol{\tau}_j)$, both the isoscalar and isovector tensor ($n = 5, 6$) and the spin-orbit ($n = 7, 8$) components. The functions $f(r)$ and $\mathcal{F}^{(n)}(r)$ depend upon several variational parameters fixed by minimizing the ground-state expectation value of the hamiltonian, $\langle H \rangle$. For $A \leq 6$ nuclei, $\langle H \rangle$ and other quantities of interest may be calculated using Monte Carlo techniques to sample the necessary many-body integrals. This is not feasible in larger nuclei and in nuclear matter. In this last system, Fermi hypernetted chain (FHNC) theory has been successfully applied [10,11]).

Recently Pieper *et al.* [12]) have performed variational calculations of the binding energy of ^{16}O with the trial wave functions (1.3) using Monte Carlo techniques. In this calculation, the scalar part of the correlation has been exactly treated, whereas the contribution of the operational components ($n > 1$) has been approximated considering up to four-body cluster terms. Guardiola *et al.* [13]) have used low-order cluster expansions to study $N = Z$ nuclei, up to ^{40}Ca, with simple central interactions and Jastrow correlation. Boscá and Guardiola [14]) have applied similar techniques to light nuclei ($A \leq 16$) using realistic interactions and state-dependent correlations.

Applying finite-order cluster-expansion techniques becomes more and more difficult and unreliable as A increases, and it is a prohibitive task for large nuclei such as ^{208}Pb. However, microscopic calculations of nuclei in this mass region are indeed most needed to have a clear understanding of the interplay between surface, shell effects and correlation effects. To this aim, the extension and the application of the FHNC theory to finite nuclei appears particularly appealing since this approach could provide the tool to overcome the technical and numerical difficulties of the variational Monte Carlo (VMC) and of the finite cluster expansion techniques.

Fantoni and Rosati [15]) originally generalized the FHNC theory with simple Jastrow correlation to treat finite Bose and Fermi systems. Later, Krotscheck *et al.* [16]) implemented and applied this theory to study surface properties of quantum liquids.

From the experience developed in nuclear-matter calculations, we know that the operatorial components of $\mathcal{F}(ij)$ are smaller than the scalar ones, and their contribution can be treated, with a good accuracy, in the single operator chain (SOC) approximation [10]). However, it should be stressed that the many-body contributions from the scalar components of the correlation function cannot be approximated with partial cluster summations, mainly when searching for the energy minimum.

The goal of this first paper is to ascertain the degree of real applicability and accuracy of the FHNC method for finite Fermi systems in dealing with central correlations. We present a detailed variational calculation of the binding energies of various $N = Z$ nuclei, for the case of state-independent Jastrow correlation operators and semi-realistic nucleon-nucleon (NN) central interactions. The distribution functions entering the calculations are evaluated by using the FHNC treatment of ref. [15]). A similar calculation was done by Krotscheck [17]) in an $A = 16$ system for the Malfliet-Tjon potential, with a simplified version of the FHNC equations.

The extension of the theory to state-dependent correlation operators, of the type used in nuclear-matter calculations, and to $N \neq Z$ nuclei will be given in a forthcoming paper.

We find that FHNC estimates agree fairly well with the available Monte Carlo results.

The plan of the paper is the following: in sect. 2 we present some technical details of the FHNC evaluation of the one-body density, of the two-body distribution

function and of $\langle H \rangle$; the results obtained for ^{4}He, ^{16}O, ^{40}Ca are presented and discussed in sect. 3, and finally, in sect. 4, we present our conclusions.

2. FHNC method

In this work we consider a variational wave function of the ground state of an $N = Z$ nucleus of the following form:

$$\Psi_0(1, 2, \ldots, A) = F(1, 2, \ldots, A)\Phi_0(1, 2, \ldots, A), \tag{2.1}$$

where $F = \prod_{i<j} f(r_{ij})$. This is equivalent to take $f_{SD} = 1$ and therefore $\mathscr{F}^{(n>1)} = 0$. The mean-field ground-state wave function $\Phi_0(1, 2, \ldots, A)$ is taken to be the Slater determinant of the single-particle wave function $\phi_\alpha(i)$,

$$\Phi_0(1, \ldots, A) = \mathscr{A}(\phi_1(1), \ldots, \phi_A(A)), \tag{2.2}$$

where $\mathscr{A}$ is the antisymmetrization operator and $\phi_\alpha(i)$ are eigenfunctions of the single-particle hamiltonian

$$h_{sp}(r) = -\frac{\hbar^2}{2m}\nabla_r^2 + U(r). \tag{2.3}$$

The more general case, with state-dependent correlations and $N \neq Z$ will be discussed in following papers.

The kinetic-energy expectation value is given by

$$\langle T \rangle \equiv -\frac{\hbar^2}{2m}\left\langle \Phi_0^* G \sum_i \nabla_i^2 G \Phi_0 \right\rangle, \tag{2.4}$$

where we have defined

$$\langle X \rangle \equiv \frac{\int d\tau X}{\int d\tau |\Psi|^2}, \tag{2.5}$$

and $\int d\tau$ indicates the integration over the spatial coordinates as well as the sum over the spin and isospin indices. We calculate $\langle T \rangle$ by using the Jackson-Feenberg transformation to eliminate terms of the form $(\nabla_i F)(\nabla_i \Phi_0)$ involving three-body operators expectation values [18]).

The resulting expression can be written as

$$\langle T \rangle = T_{JF} = T_F + T_\phi, \tag{2.6}$$

where

$$T_F \equiv -\frac{\hbar^2}{4m}\left\langle \Phi_0^* \left(F \sum_i (\nabla_i^2 F) - \sum_i (\nabla_i F)^2 \right) \Phi_0 \right\rangle, \tag{2.7}$$

and

$$T_\phi \equiv -\frac{\hbar^2}{4m}\left(\left\langle \Phi_0^* F^2 \sum_i \nabla_i^2 \Phi_0 \right\rangle - \sum_i \langle (\nabla_i \Phi_0^*) F^2 (\nabla_i \Phi_0) \rangle \right). \tag{2.8}$$

The two-body potential expectation value is given by

$$\langle v\rangle = \left\langle \Psi_0^* \sum_{i<j} v(ij)\Psi_0 \right\rangle. \tag{2.9}$$

The tensor and the spin-orbit components of the two-body potential give vanishing contribution for spin-isospin saturated systems when pure Jastrow correlations are used. Therefore, in this first analysis, it is more consistent to consider nucleon-nucleon interactions of a central type (v_4 interaction), namely

$$v(ij) \equiv \sum_{n=1,4} v^{(n)}(r_{ij}) O^{(n)}(i,j). \tag{2.10}$$

The FHNC theory allows to calculate the expectation values (2.7)-(2.9) performing an expansion in power series of the function

$$h(r) = f^2(r) - 1. \tag{2.11}$$

The product form of the correlation in eq. (2.1) generates *cluster terms* characterized by both the number of particles and the number of the dynamical correlations $h(r_{ij})$ linking the particles. In addition, each n-body cluster may contain *statistical correlations* generated by the Pauli principle.

It is worth noting that both the numerator and the denumerator of $\langle X\rangle$ contain a finite number of cluster diagrams. By developing this ratio in powers of h, we get an infinite series of cluster terms [15]) whose properties will be summarized in the following.

The FHNC theory sums to all orders the various cluster terms by using the integral-equation method.

2.1. DISTRIBUTION FUNCTIONS

The key quantities entering the calculation of $\langle H\rangle = \langle \Psi_0^* H \Psi_0\rangle$ are the one- and two-body distribution functions

$$\rho_1(r_1) \equiv \rho(r_1) \equiv \left\langle \Psi_0^* \sum_i \delta(r_1 - r_1)\Psi_0 \right\rangle, \tag{2.12}$$

$$\rho_2^{(n\leq 4)}(r_1, r_2) \equiv \left\langle \Psi_0^* \sum_{i\neq j} \delta(r_1 - r_i)\delta(r_2 - r_j) O^{(n)}(i,j)\Psi_0 \right\rangle. \tag{2.13}$$

In fact the r.h.s. of eqs. (2.7)-(2.9) can always be expressed in terms of the FHNC quantities entering the evaluation of the distribution functions.

We will now outline the procedure to calculate the distribution functions within the FHNC theory. A more complete description of the FHNC theory can be found in ref. [15]).

The clusters contributing to $\rho_2^{(n)}(r_1, r_2)$ are most conveniently represented by diagrams, hereafter denoted as two-point renormalized FHNC diagrams (RFHNC),

in order to distinguish them from the standard FHNC diagrams encountered in the case of translationally invariant many-body systems, as nuclear matter or liquid helium. A few examples of RFHNC diagrams are given in fig. 1.

The RFHNC diagrams, besides the two *external points* 1 and 2, representing the arguments of $\rho_2^{(n)}(r_1, r_2)$, may have any number of *internal points* ($i \neq 1, 2$), irrespective of the mass number A of the considered nucleus. The label i stands for both the coordinate r_i and the spin-isospin assignments $\chi_s(i)\chi_t(i)$ of the particle i. For each internal point i, the integration over r_i and the summation over spin-isospin states are implied.

The points are joined either by *dynamical correlations* (h-bonds), which are graphically represented by a dashed line, or by *exchange links* (e-bonds), drawn as oriented solid lines and representing the uncorrelated density matrix

$$n_0(i,j) \equiv \rho_0(r_i, r_j) = \sum_{\alpha \cdots \alpha_A} \phi_\alpha^*(i)\phi_\alpha(j) = \sum_{ss't} \chi_s^*(i)\chi_t^*(i)\chi_{s'}(j)\chi_t(j)\rho_{ss'}^t(r_i, r_j), \quad (2.14)$$

where the sum on α is extended to the $\frac{1}{4}A$ states of the Fermi sea of the A-nucleus considered.

The diagonal part of eq. (2.14) is

$$n_0(i) \equiv \rho_0(r_i) = \sum_{\alpha \cdots \alpha_A} |\phi_\alpha(i)|^2, \quad (2.15)$$

and gives the uncorrelated one-body distribution function. It should be graphically

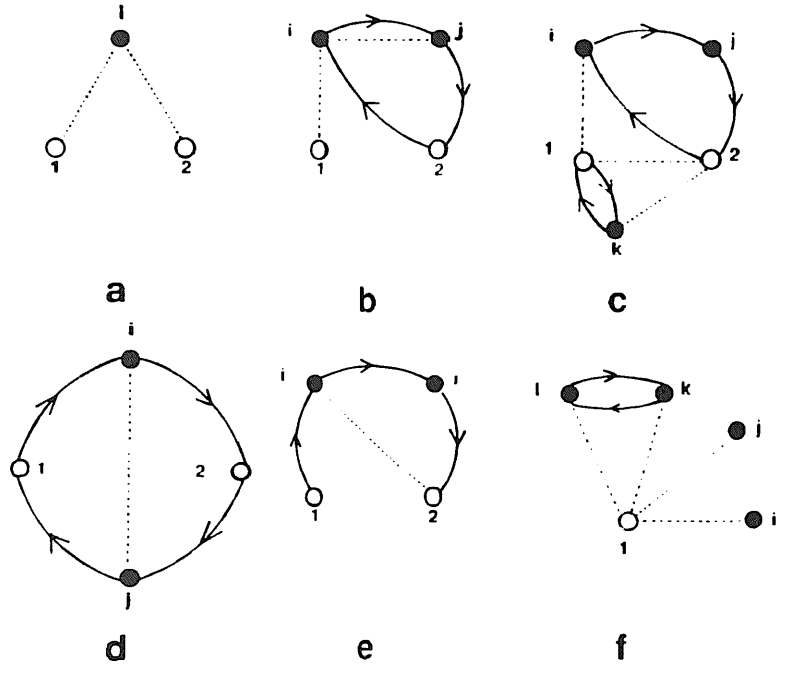

Fig. 1. A few examples of cluster diagrams contributing to the distribution functions. A dashed line stands for the dynamical correlation $h(i,j)$ and an oriented solid line for the statistical correlation $\rho_0(i,j)$. A black dot associated with a point, implies integration over its coordinates.

represented by a one-point exchange loop but, for the sake of simplicity, we have omitted it in fig. 1.

If the $|l^2 s^2 l_z s_z\rangle$ representation is used for the single-particle orbitals, the exchange function $\rho^l_{ss'}$ is not only diagonal in the spin variables but also independent on them. The isospin dependence comes on account of the fact that different single-particle orbitals for neutrons or protons might be allowed for. We consider $N = Z$ and assume the neutrons and protons single-particle states being the same, so the exchange function is spin-isospin independent. Its explicit expression is given in appendix B.

The RFHNC diagrams are constructed by following the rules given below:

(a) there are no isolated points: the external points 1 and 2 must be reached by at least one bond and the internal points $i \neq 1, 2$ by at least two bonds;

(b) the e-bonds are arranged in closed loops with no common points, each carrying a factor $2(-1)^{n-1}$, n being the number of points in the loop. The only exception comes from the two-point loop, carrying a factor (-1), instead of (-2);

(c) as a result of rule (b), a given point i can be reached by at most two e-bonds. On the contrary, there is no limitation on the number of h-bonds reaching a given point. Any pair of points i and j can be joined by at most one h-bond;

(d) each point i carries a vertex correction function $\xi(r_i)$. There are three types of points and correspondingly three different vertex corrections:

(i) type d points are reached by dynamical correlations only and are vertex corrected by $\xi_d(r_i)$, which coincides with the one-body distribution function $\rho(r_i)$;

(ii) type e points are reached by an exchange loop and, if they are internal points, by at least one h-bond. They are vertex corrected by $\xi_e(r_i)$;

(iii) type p points belong to an exchange (or permutation) loop and are not reached by any h-bond. Their vertex correction is denoted with $\xi_p(r_i)$ and it is given by

$$\xi_p(r_i) = \xi_e(r_i) - 1 , \tag{2.16}$$

where the factor 1 is subtracted because diagrams where the point i is not reached by any h-bond are strictly prohibited. In fact, the subtraction of the factor 1 from $\xi_e(r_i)$ implies that $\xi_p(r_i)$ vanishes in the limit of the uncorrelated wave function $[h(r) = 0]$. The external points can be either of type d or of type e;

(e) the only pre-factor of a RFHNC diagram is the so-called symmetry factor $1/\mathcal{P}$, where $\mathcal{P}$ is the number of permutations of the internal points leaving unchanged the corresponding cluster term;

(f) the RFHNC diagrams must be irreducible.

The diagrams are grouped according to the exchange character of the external points: *dd*, *de*, *ed* and *ee*. There are also c-c diagrams i.e. diagrams where each external point is reached by a single exchange line. A further classification of the RFHNC diagrams, which will be used throughout the paper, distinguishes the diagrams in nodal ($N_{\alpha\beta}$), composite ($X_{\alpha\beta}$) and elementary ($E_{\alpha\beta}$), see appendix A.

The FHNC theory enables one to evaluate and sum, up to infinite order, the diagrams belonging to the various groups, by solving a set of coupled integral equations. These equations are reported in appendix A.

The one-body distribution function, and the vertex correction functions have the following structure,

$$\rho_1(r_1) \equiv \xi_d(r_1) = [\rho_0(r_1) + U_e(r_1)] \exp[U_d(r_1)], \tag{2.17}$$

and

$$\xi_e(r_1) = \exp[U_d(r_1)], \tag{2.18}$$

where the FHNC quantities $U_d(r_1)$ and $U_e(r_1)$ are the sums of the one-point RFHNC diagrams in which the external point 1 is of type d or e, respectively. Notice that, on account of rule (b), if a given point i of a diagram is of type e, then its vertex correction $\xi_e(r_i)$ must include one-point diagrams in which the external point is of type d. There is no such a limitation for $\xi_d(r_i)$, which in fact coincides with the full one-body distribution function. For instance the diagram 1f of fig. 1 is included in $\xi_e(r_i)$ and the functions associated with the two different branches of the diagrams ($1-i$ or $1-j$ and $1-kl$) are contained in $U_d(r_1)$.

For the two-body distribution functions we find the expression

$$\rho_2^{(1)}(r_1, r_2) = \rho_1(r_1)\rho_1(r_2)g_{dd}(r_1, r_2) + \rho_1(r_1)\xi_e(r_2)g_{de}(r_1, r_2) + \xi_e(r_1)\rho_1(r_2)g_{ed}(r_1, r_2)$$
$$+ \xi_e(r_1)\xi_e(r_2)[g_{ee}^{dir}(r_1, r_2) + g_{ee}^{exch}(r_1, r_2)], \tag{2.19}$$

and

$$\rho_2^{(n-1)}(r_1, r_2) = a_n \xi_e(r_1)\xi_e(r_2)g_{ee}^{exch}(r_1, r_2), \tag{2.20}$$

with $a_n = 3, 3, 9$ for $n = 2, 3, 4$, respectively. Only the diagrams of the exchange type, characterized by the two external points 1 and 2 belonging to the same exchange loop, as in diagram 1d, contribute to $\rho_2^{(n-1)}(r_1, r_2)$ in a spin-isospin saturated system and for state-independent correlations.

The partial distribution functions g_{dd}, g_{de}, g_{ed} and g_{ee} sum up the RFHNC diagrams of the type specified by the subscripts (see diagrams $1a \in g_{dd}$, $1b \in g_{de}$, 1c and $1d \in g_{ee}$). Their expressions are given in appendix A together with the expressions of U_d and U_e.

2.2. ENERGY EXPECTATION VALUE

The evaluation of the energy mean value leads to the following expression for T_G:

$$T_F = -\frac{\hbar^2}{4m} \int d^3r_1\, d^3r_2\, \rho_2^{(1)}(r_1, r_2) t[f(r_{12})], \tag{2.21}$$

where

$$t[f(r_{12})] \equiv \frac{1}{f^2(r_{12})}\left(f(r_{12})f''(r_{12}) + \frac{2}{r_{12}}f(r_{12})f'(r_{12}) - f'^2(r_{12})\right). \tag{2.22}$$

The cluster expansion of T_ϕ [eq. (2.8)] is obtained by following the same procedure used for the corresponding kinetic-energy term of nuclear matter [15]). Three different types of cluster terms must be distinguished, leading to

$$T_\phi = T_\phi^{(1)} + T_\phi^{(2)} + T_\phi^{(3)}, \tag{2.23}$$

where the evaluation of the generic term $T_\phi^{(n)}$ requires the use of n-body distribution functions.

The term $T_\phi^{(1)}$ sums the cluster diagrams in which the external point 1 [on which ∇_1 is acting and associated with the dummy label i in eq. (2.8)] is not involved in any exchange. The resulting expression is

$$T_\phi^{(1)} = -\frac{\hbar^2}{4m}\int \mathrm{d}^3 r_1\, \rho_{T1}(r_1)\xi_e(r_1), \tag{2.24}$$

where ρ_{T1} is defined as

$$\rho_{T1}(r_1) = \sum_\alpha \phi_\alpha^*(r_1)\nabla_1^2\phi_\alpha(r_1) - \sum_\alpha \nabla_1\phi_\alpha^*(r_1)\cdot\nabla_1\phi_\alpha(r_1). \tag{2.25}$$

When the external point 1 is involved in an exchange loop, it is necessary to distinguish the case of the two-point from the $n(>2)$-point loop, leading to $T_\phi^{(2)}$ and to $T_\phi^{(3)}$, respectively. $T_\phi^{(2)}$ is given by

$$T_\phi^{(2)} = \frac{\hbar^2}{4m}\int \mathrm{d}^3 r_1\, \mathrm{d}^3 r_2\, \xi_e(r_1)\rho_{T2}(r_1, r_2)\{[g_{dd}(r_1, r_2) - 1]\xi_e(r_2) + \xi_p(r_2)\}, \tag{2.26}$$

where

$$\rho_{T2}(r_1, r_2) = \rho_0^\dagger(r_1, r_2)\nabla_1^2\rho_0(r_1, r_2) - \nabla_1\rho_0^\dagger(r_1, r_2)\cdot\nabla_1\rho_0(r_1, r_2). \tag{2.27}$$

The evaluation of $T_\phi^{(3)}$ requires, in principle, the knowledge of a three-particle distribution function. However, as in the case of nuclear matter, the leading term of $T_\phi^{(3)}$ in eq. (2.8) is $\phi^*\nabla_i^2\phi$, leading to two-point RFHNC diagrams, in which the two-body exchange link

$$\rho_{T3}(r_1, r_2) = \frac{1}{\nu}\sum_{st}\chi_s^\dagger(2)\chi_t^\dagger(2)\nabla_1^2\rho_0(r_1, r_2)\chi_s(1)\chi_t(1) \tag{2.28}$$

closes the appropriate exchange loops summed by the FHNC functions of the *cc* type (see appendix A). The final expression for $T_\phi^{(3)}$ is

$$T_\phi^{(3)} = T_\phi^{(3,2)} + T_\phi^{(3,3)}, \tag{2.29}$$

where

$$T_{\phi}^{(3,2)} = -\frac{\hbar^2}{4m} 2\nu \int d^3r_1\, d^3r_2\, \rho_{T3}(r_1, r_2)\xi_e(r_1)$$
$$\times (\xi_e(r_2)\{[g_{dd}(r_1, r_2) - 1]N_{cc}(r_1, r_2) + N_{cc}^{xx}(r_1, r_2) + N_{cc}^{px}(r_1, r_2)\}$$
$$+ \xi_p(r_1)[N_{cc}^{xp}(r_1, r_2) + N_{cc}^{pp}(r_1, r_2)]$$
$$+ \xi_e(r_2) g_{dd}(r_1, r_2) E_{cc}(r_1, r_2)\}, \tag{2.30}$$

ν being the degeneracy number and N_{cc}, $N_{cc}^{\alpha,\beta}(\alpha, \beta = x, p)$ and E_{cc} are the sums of the *cc* nodal and elementary diagrams described in appendix A.

The term $\nabla_i\phi^* \cdot \nabla_i\phi$ in eq. (2.8) leads to $T_{\phi}^{(3,3)}$, containing the three-body operator $\nabla_1\rho_0^{\dagger}(r_1, r_3) \cdot \nabla_1\rho_0(r_1, r_2)$. This term has been verified to be very small in nuclear matter [8]) and therefore is neglected in the present calculation.

The center-of-mass kinetic energy, $T_{c.m.}$, given by

$$T_{c.m.} = -\frac{\hbar^2}{2mA}\left\langle \Psi_0^* \left(\sum_i \nabla_i\right)^2 \Psi_0 \right\rangle, \tag{2.31}$$

must be subtracted from $\langle T + V\rangle$ to get the energy mean value $\langle E\rangle = \langle H\rangle - T_{c.m.}$. $T_{c.m.}$ is written as

$$T_{c.m.} = -\frac{\hbar^2}{4mA}\left(\int d^3r_1\, \rho_{T1}(r_1) - \int d^3r_1\, d^3r_2\, \rho_{T4}(r_1, r_2)\right), \tag{2.32}$$

where the density $\rho_{T4}(r_1, r_2)$ is defined as

$$\rho_{T4}(r_1, r_2) \equiv -\rho_0^{\dagger}(r_1, r_2)\nabla_1 \cdot \nabla_2\rho_0(r_1, r_2) + \nabla_1\rho_0^{\dagger}(r_1, r_2) \cdot \nabla_2\rho_0(r_1, r_2). \tag{2.33}$$

The explicit expressions for $\rho, \rho_{T1}, \ldots, \rho_{T4}$ are given in appendix B. In the case of an harmonic-oscillator single-particle potential U with parameter ω, eq. (2.33) gives the well-known result $T_{c.m.} = \frac{3}{4}\hbar\omega$. The final expression for $\langle E\rangle$ is

$$\langle E\rangle = T_F + T_{\phi} - T_{c.m.} + \tfrac{1}{2}\int d^3r_1\, d^3r_2 \left(\rho_2^{(1)}(r_1, r_2)v^{(1)}(r_{12})\right.$$
$$\left. - \nu \sum_{n=2}^{4} v^{(n)}(r_1, r_2)\rho_2^{(n)}(r_1, r_2)\right). \tag{2.34}$$

3. Results

The best variational choices for both $f(r)$ and the single-particle wave functions $\phi_\alpha(r_\alpha)$ are obtained by solving the Euler equations $[\delta\langle H\rangle/\delta f(r)] = 0$ and $[\delta\langle H\rangle/\delta\phi_\alpha(r_\alpha)] = 0$ [ref. [17])]. An approximated solution of these equations can be numerically obtained in the case of pure Jastrow correlations [17]), but it becomes a prohibitive task when realistic nucleon-nucleon interactions and correlations are

considered. An alternative procedure consists in parametrizing the wave functions and minimizing $\langle H \rangle$ with respect to the variational parameters.

We have followed the latter procedure and we have generated the single-particle wave functions ϕ_α with two different mean fields: the harmonic-oscillator well characterized by oscillator length $b = \sqrt{\hbar/m\omega}$, and a Woods-Saxon well ($U_{\rm WS}$) of the form

$$U_{\rm WS}(r) = \frac{U_0}{1+\exp[(r-R)/a]}, \tag{3.1}$$

where U_0, R, a are the variational parameters for the Woods-Saxon well and b for the harmonic oscillator.

We have used correlation functions $f(r)$ of the simple gaussian form

$$f_{\rm G}(r) = 1 + \alpha \exp(-\beta r^2), \tag{3.2}$$

or $f_{\rm Eul}(r)$ determined by minimizing the lowest-order cluster expansion $\langle H_2 \rangle$ of $\langle H \rangle$, given by

$$\langle H_2 \rangle = -\frac{\hbar^2}{4m} \int \mathrm{d}^3 r_1 \, \rho_{T1}(r_1) + \int \mathrm{d}^3 r_1 \, \mathrm{d}^3 r_2 \, \{Q(r_1, r_2) - P(r_1, r_2)[f(r_{12})\nabla^2 f(r_{12}) - f'^2(r_{12})]\}, \tag{3.3}$$

where

$$Q(r_1, r_2) = \frac{\hbar^2}{4m} \rho_{T2}(r_1, r_2)[f^2(r_{12}) - 1] + \tfrac{1}{2}[\rho_0(r_1)\rho_0(r_2) - \rho_0^2(r_1, r_2)] f^2(r_{12}) v^{(1)}(r_{12}) - \tfrac{1}{2}\nu[3v^{(2)}(r_{12}) + 3v^{(3)}(r_{12}) + 9v^{(4)}(r_{12})]\rho_0^2(r_1, r_2) f^2(r_{12}), \tag{3.4}$$

and

$$P(r_1, r_2) = \frac{\hbar^2}{4m}[\rho_0(r_1)\rho_0(r_2) - \nu\rho_0^2(r_1, r_2)], \tag{3.5}$$

under the constraints

$$f(r \geq 1) = 1, \quad \text{and} \quad f'(r \geq d) = 0,$$

with the healing distance d being a variational parameter.

The minimization is achieved by solving the following Euler-Lagrange equation:

$$u''(r) - \tilde{V}(r)u(r) = \lambda u(r), \tag{3.6}$$

where we have defined

$$u(r) = r\sqrt{\bar{P}(r)}\, f(r)\,, \tag{3.7}$$

$$\tilde{V}(r) = \left(\nabla^2 \bar{P}(r) + 2\bar{Q}(r) - \frac{\bar{P}'(r)^2}{\bar{P}(r)}\right)\frac{1}{4\bar{P}(r)}, \tag{3.8}$$

with the constraints

$$u(d) = d\sqrt{\bar{P}(d)}\,, \qquad u'(d) = \frac{2[\bar{P}(d) + d\bar{P}'(d)]}{2\sqrt{\bar{P}(d)}}\,. \tag{3.9}$$

The quantities $\bar{P}$ and $\bar{Q}$ are obtained by integrating $P(r_1, r_2)$ and $Q(r_1, r_2)$ over r_1 and r_2 and keeping the interparticle distance r_{12} fixed, namely

$$\bar{X}(r) = \frac{1}{r_{12}} \int_0^\infty r_1\, dr_1 \int_{|r_{12}-r_1|}^{r_1+r_{12}} r_2\, dr_2\, X(r_1, r_2, r_{12})\,, \tag{3.10}$$

where X can be either P or Q.

In this way we obtain a parametrization of the correlation function $f(r)$ very efficient in reproducing the short-range behavior of the optimal $f(r)$. Moreover, this scheme is readily generalizable to the case of state-dependent correlations and to a mean-field potential which includes isospin and spin-orbit dependence.

In order to test the accuracy of the FHNC scheme in treating the strong nucleon-nucleon correlations, we have considered nucleon-nucleon central potentials which are strongly repulsive at short distances and have been used in previous calculations in complex nuclei.

The first interaction we have used is the spin-isospin independent Malfliet-Tjon potential [19]) (v_{MT}), which has been used in variational Monte Carlo (VMC), Green function Monte Carlo (GFMC) [6]) and FHNC/c [17]) calculations of ^{16}O. This interaction does not saturate nuclear matter and leads to unphysically dense nuclei and has been considered only for the sake of comparison with previous calculations.

The second interaction we have used is the Brink-Boeker B1 central potential (v_{B1}) [20]). It is an effective nucleon-nucleon interaction, since it does not fit the two-body data, and it is determined in such a way to reproduce both nuclear matter and ^{4}He binding energies in Hartree-Fock theory. It has been used in VMC calculations of ^{16}O [refs. [21,22])].

We have also considered the semi-realistic central interaction S3 by Afnan and Tang [23]) (v_{S3}). It reproduces the s-wave two-body scattering data up to roughly 60 MeV; it provides reasonable value of the binding energies and of the radii of the $A = 3, 4$ nuclei and an equation of state of nuclear matter which is not too different from those obtained with realistic two-body interactions. Since the original S3 potential is only defined for two-particle states of even parity, analogously to what has been done in ref. [13]), we supplemented the potential in the odd channels with a repulsive interaction given by the repulsive term of the even channels.

In addition to the binding energies and the one-body density $\rho_1(r)$, particular attention has been also devoted to the normalization sum rules:

$$S_1 = \frac{1}{A}\int d^3r\, \rho_1(r) = 1\,, \tag{3.11a}$$

$$S_2 = \frac{1}{A(A-1)}\int d^3r_1\, d^3r_2\, \rho_2^{(1)}(r_1, r_2) = 1\,, \tag{3.11b}$$

and

$$S_\sigma = \frac{1}{3A}\int d^3r_1\, d^3r_2\, \rho_2^{(n=2,3)}(r_1, r_2) = -1\,, \tag{3.11c}$$

which provide useful information on the accuracy of the approximations used to solve the FHNC equations. The sum rule (3.11c) holds only in a spin-isospin saturated system.

The sums, at all orders, of the nodal $N_{\alpha\beta}$ and composite $X_{\alpha\beta}$ diagrams (see appendix A) can be expressed in a closed form through the FHNC equations, once the sum of the elementary diagrams $E_{\alpha\beta}$ is given. Unfortunately, no exact method to evaluate the elementary contribution has been devised so far, so one has to use approximations to estimate $E_{\alpha\beta}$.

The simplest approximation consists in setting $E_{\alpha\beta} = 0$ (FHNC/0 approximation). This is the approximation used in most of the calculations of the equations of state of nuclear and neutron matter [8]. These studies indicate that the elementary diagrams give very little contribution in the case of translationaliy invariant nuclear systems, when realistic nucleon–nucleon interactions are used.

A better level of approximations is obtained by including the most important elementary diagrams. The well-known FHNC/4 approximation includes only the lowest-order elementary diagrams $E_{\alpha\beta}/4$, i.e. those originated by four particle clusters (see fig. 1d).

We tested the validity of the FHNC/0 approximation comparing our results of the ground-state properties of an ^{16}O nucleus interacting via the Malfliet-Tjon potential with the VMC calculations of ref. [6]). The calculation has been performed with the same single-particle wave functions of ref. [6]) generated by a Woods-Saxon potential with parameters $U_0 = -207$ MeV, $a = 0.5$ fm and $R = 1$ fm. We used the correlation function $f_{\mathrm{Eul}}(r)$, solution of eq. (3.6) with the same value of the healing distance ($d = 2$ fm), used in ref. [6]). We obtained for the binding energy the value $\langle H\rangle_{\mathrm{FHNC/0}} = -987$ MeV, to be compared with the VMC result $\langle H\rangle_{\mathrm{VMC}} = -1024 \pm 5$ MeV. Also the results obtained for the sum rules give us confidence about the validity of FHNC/0. The sum rules S_1 and S_2 are satisfied within less than 1%, whereas $S_\sigma = -1.030$.

A calculation of the ground-state properties of the ^{16}O nucleus interacting with a Malfliet-Tjon potential within the framework of the FHNC/c approximation has

been done by Krotscheck [17]), who uses a correlation function obtained by solving $\delta\langle H\rangle_{\mathrm{FHNC}/c}/\delta f(r)=0$, and a set of Woods-Saxon parameters ($U_0=-310$ MeV, $a=0.6$ fm, and $R=1.86$ fm) reproducing the r.m.s. radius of the GFMC calculation of ref. [6]). With the same set of parameters, and using $f_{\mathrm{Eul}}(r)$ with $d=2$ fm, we obtained for the binding energy of ^{16}O the value of $\langle H\rangle_{\mathrm{FHNC}/0}=-1152$ MeV to be compared with $\langle H\rangle_{\mathrm{ref.}[17]}=-1055$ MeV. A marginally better energy ($\langle H\rangle=-1059$ MeV) has been obtained in ref. [17]) employing the single-particle wave functions coming from $\delta\langle H\rangle_{\mathrm{FHNC}/c}/\delta\phi_\alpha(r)=0$. The GFMC result of ref. [6]) is $\langle H\rangle_{\mathrm{GFMC}}=-1194\pm20$ MeV. The one-body distribution function $\rho_1(r)$ we have obtained is practically indistinguishable from that of ref. [17]).

The results presented above indicate that the FHNC/0 approximation is very accurate. In fact, from the comparison of the FHNC/0 with the Monte Carlo results it comes out that the contribution of the elementary diagrams is small, especially in view of the fact that in the considered model nucleus the central density is unphysically high [$\rho_1(0)=1.21$ fm^{-3}] and the importance of the elementary diagrams is known to increase rapidly with the density of the system.

On the other hand, one has to be careful in drawing this conclusion, because the purely scalar character of the Malfliet-Tjon potential may mask the effect of the elementary diagrams of the exchange type. In fact, sum rule (3.11c) is not satisfied with the same level of accuracy as the others and this is a signature of the importance of these diagrams.

The explicit FHNC expression of $\rho_2^{(n>1)}$ in eq. (3.11c) reads

$$\rho_2^{(n>1)}(r_1,r_2)=a_n\xi_{\mathrm{e}}(r_1)\xi_{\mathrm{e}}(r_2)g_{\mathrm{dd}}(r_1,r_2)\times\{-\nu[N_{\mathrm{cc}}(r_1,r_2)+E_{\mathrm{cc}}(r_1,r_2)-\rho_{\mathrm{o}}(r_1,r_2)]^2+E_{\mathrm{ee}}^{\mathrm{exch}}(r_1,r_2)\}\,, \tag{3.12}$$

$E_{\mathrm{ee}}^{\mathrm{exch}}$ being the sum of the *ee* elementary diagrams whose external points (1, 2) belong to the same exchange loop. It can be shown that, performing the expansion of S_σ in power series of the function h (eq. 2.11), the sum rule (3.11c) is fulfilled at each order in h. The FHNC/0 approximation cannot satisfy this sum rule since the elementary diagrams are disregarded, and, already at the first order in h, the diagram $E^{(1)}$ (shown in fig. 1d), belonging to $E_{\mathrm{ee}}^{\mathrm{exch}}$, appears. We have explicitly calculated the correction to the sum rule due to this diagram and we found the value $S_\sigma=-0.998$, largely improved with respect to the FHNC/0 value.

The validity of the FHNC/0 approximation and the role of the elementary diagrams is better studied with potentials having spin and isospin dependence. The Majorana term of the potential is particularly sensitive to the exchange part of the distribution function $\rho_2(r_1,r_2)$. For central v_4 potentials, the expectation value of the Majorana part is given by

$$\langle v_{\mathrm{M}}\rangle=\tfrac{1}{2}\int \mathrm{d}^3r_1\,\mathrm{d}^3r_2\,v^{(4)}(r_{12})\sum_{n\geq1}\rho_2^{(n)}(r_1,r_2)\,. \tag{3.13}$$

The B1 potential is a Wigner–Majorana admixture with a large Majorana part. Using this potential, we have calculated the binding energies of ^{4}He, ^{16}O and ^{40}Ca with harmonic-oscillator single-particle wave functions and with correlation functions of both gaussian and $f_{\rm Eul}(r)$ forms. In table 1 we compare our results obtained with the gaussian correlation function $f_{\rm G}(r)$ to the VMC results available for ^{4}He and ^{16}O, and, in the case of ^{40}Ca, to the results of the low-order cluster expansion FAHT/III [13]). The first row for each nucleus lists the FHNC/0 results. The second row reports the results obtained in FHNC-1 approximation, and the third row gives the VMC or the FAHT/III results.

The FHNC-1 approximation consists in adding to $v_{\rm M}$ the dressed $E^{(1)}$ diagram obtained from the diagram of fig. 1d by inserting $g_{\rm dd}$ in each exchange line and substituting h with $g_{\rm dd}-1$ between the internal points (i,j). The contribution of $E^{(1)}$ to the $v_{\rm W}$ term and to the kinetic energy has been found to be negligible.

In ^{4}He and ^{16}O the expectation values of both Wigner potential and kinetic energy are in good agreement with the VMC results and the sum rules S_1 and S_2 are very well satisfied. This makes us confident that the FHNC/0 treatment of the Jastrow correlations is rather accurate. However, for both S_{σ} and $v_{\rm M}$ a more accurate treatment of the statistical correlations is needed. The inclusion of $E^{(1)}$ brings the FHNC estimates very close to the VMC results, and S_{σ} is satisfied within less than 1%.

The result displayed in fig. 2 for the one-body density of ^{15}O shows the good agreement with the VMC calculation of ref. [22]). In the same figure we present also the uncorrelated density $\rho_0(r)$ to stress the effect of the short-range correlations.

TABLE 1

Ground-state expectation values for ^{4}He, ^{16}O and ^{40}Ca nuclei for the B1 potential, with harmonic-oscillator single-particle wave functions and gaussian correlations $f_{\rm G}$. The parameters are: $\alpha=-0.48$ (^{4}He), -0.51 (^{16}O), -0.53 (^{40}Ca); $\beta({\rm fm}^{-2})=1.56$ (^{4}He), 1.52 (^{16}O), 1.60 (^{40}Ca); $b({\rm fm})=1.231$ (^{4}He), 1.543 (^{16}O), 1.667 (^{40}Ca). We list the expectation values of the Majorana and Wigner ($\langle v_{\rm M}\rangle$ and $\langle v_{\rm W}\rangle$) potentials, of the kinetic energy ($\langle T\rangle$), of the center-of-mass contribution $T_{\rm c.m.}$, and of the energy ($\langle E\rangle$). All the energies are expressed in MeV. The VMC results are from ref. [21]) (the errors are $\sim\pm0.2$ MeV); the FAHT/III results are from ref. [13])

Nucleus	Theory	$\langle v_{\rm M}\rangle$	$\langle v_{\rm W}\rangle$	$\langle T\rangle$	$T_{\rm c.m.}$	$\langle E\rangle$
^{4}He	FHNC/0	−132.5	24.5	83.9	20.5	−44.5
	FHNC-1	−125.6				−37.7
	VMC	−123.8	24.8	83.0		−36.4
^{16}O	FHNC/0	−421.6	−63.3	329.8	13.1	−168.2
	FHNC-1	−403.8				−150.4
	VMC	−402.6	−62.3	327.1		−150.9
^{40}Ca	FHNC/0	−1084	−387	964	11	−518
	FHNC-1	−1035				−471
	FAHT/III					−478

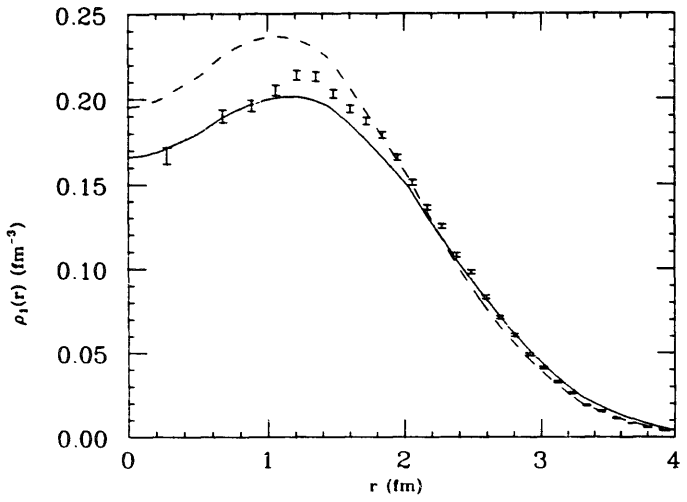

Fig. 2. Density of ^{16}O calculated with the B1 potential, harmonic-oscillator single-particle wave functions and gaussian correlation (see text). The points with vertical error bars show the VMC results of ref. [22]). The dashed line is the uncorrelated one-body density $\rho_0(r)$.

In absence of VMC calculations for ^{40}Ca, we compare, in table 1, our results with those of ref. [13]) obtained within the FAHT/III approximation. Our result differs from the FAHT/III calculation of ref. [13]) of about 0.5 MeV per nucleon. This is consistent with the results of ref. [21]) in ^{16}O, where the same difference has been found between VMC and FAHT/III.

With the same harmonic-oscillator mean fields used in table 1, we have repeated the calculations with the correlation $f_{\mathrm{Eul}}(r)$ discussed at the beginning of the section. These calculations have been performed to test the FHNC method with a class of trial wave functions and correlations which will be used in conjunction with realistic nucleon–nucleon interactions. The results are given in table 2 and they are compared with the VMC energies [24]). As in the previous case the FHNC results to be a fully reliable approximation. The binding energies obtained with $f_{\mathrm{Eul}}(r)$ are slightly lower

TABLE 2

Ground-state properties of ^{4}He, ^{16}O and ^{40}Ca nuclei for the B1 potential, with harmonic-oscillator wave functions and Euler correlation f_{Eul}. The energies are expressed in MeV and the lengths in fm. The parameters of the harmonic oscillator are the same as in table 1. The VMC results are from ref. [24]).

Nucleus	Theory	$\langle v_{\mathrm{M}} \rangle$	$\langle v_{\mathrm{W}} \rangle$	$\langle T \rangle$	$T_{\mathrm{c.m.}}$	$\langle E \rangle$	d
^{4}He	FHNC/0	−126.6	17.3	84.7	20.5	−45.1	2.20
	FHNC-1	−119.4				−37.9	
^{16}O	FHNC/0	−435.4	−49.1	330.0	13.1	−167.2	2.04
	FHNC-1	−420.2				−152.4	
	VMC	−417.2	−49.9	328.4		−151.8	
^{40}Ca	FHNC/0	−1108	−354	953	11	−520	1.96
	FHNC-1	−1070				−482	

TABLE 3

Ground-state properties of ^{16}O and ^{40}Ca nuclei for the S3 potential, with harmonic-oscillator single-particle wave functions and Euler correlations f_{Eul}. The harmonic-oscillator parameters are: $b_{h.o.}$(fm) = 1.538(^{16}O), 1.654(^{40}Ca). The energies are expressed in MeV and the lengths in fm.

Nucleus	Theory	$\langle v \rangle$	$\langle T \rangle$	$T_{c.m.}$	$\langle E \rangle$	d
^{16}O	FHNC/0	−479.1	378.7	13.2	−113.5	2.08
	FHNC-1	−470.8			−105.3	
^{40}Ca	FHNC/0	−1483	1124	11	−370	2.12
	FHNC-1	−1463			−350	

than the corresponding results for the gaussian correlation. We have not performed a full minimization varying the harmonic-oscillator parameters or using a Woods-Saxon well, which would result in a further lowering of the energy. This investigation will be a subject of a future study.

We have finally considered the S3 potential as an example of semi-realistic nucleon-nucleon interaction, which is closer to a realistic interaction as far as the short-range repulsion is concerned. We did not find peculiar differences with respect to the previous cases. The results for ^{16}O and ^{40}Ca are shown in table 3. It should be noticed that the contribution of the $E^{(1)}$ term is always of the same magnitude, independently on the used interaction. FHNC-1 appears to be a realiable approximation. We have also computed the binding energy of ^4He with $b = 1.22$ fm and gaussian correlation, with $\alpha = -0.725$ and $\beta = 2.1$ fm^{-2} and compared with the available VMC result [25]). We obtained for the energy of ^4He the value of −24.7 MeV to be compared with $\langle H \rangle_{VMC} = -23.9$ MeV.

4. Conclusions

This work is the first step towards a description of medium-heavy nuclei, such as ^{40}Ca and ^{208}Pb, with correlated wave functions of the type extensively used in nuclear matter. In fact, exact techniques for solving the many-body Schrödinger equation, like Fadeev or GFMC, are at present applicable in light systems only.

In this paper we have presented the basic formulation to apply CBF theory to complex nuclei, and we have performed some numerical calculations to test the validity of our approach.

We have developed a new FHNC scheme, named FHNC-1, which is able to treat at a satisfactory level of accuracy the state-independent part of the nucleon-nucleon correlation. This is known to be the part of the correlation which needs to be treated with the highest possible accuracy. The FHNC-1 scheme consists in adding to the FHNC/0 approximation for finite systems the leading elementary diagram of the exchange type, which is the only one contributing to the first order of the power-series cluster expansion.

We have calculated the binding energy of ^{4}He, ^{16}O and ^{40}Ca. There is a very good agreement between FHNC-1 estimates and the available VMC results. FHNC/0 has been found reliable enough for calculating the expectation values of scalar operators. In fact it provides very good results for the Malfliet-Tjon potential as well as for $\langle T \rangle$ and $\langle v_W \rangle$ for all the cases considered. Moreover, sum rules S_1, S_2 are very well satisfied within the FHNC/0 approximation.

On the contrary, the expectation values of spin- and isospin-dependent operators, such as the Majorana part of the interaction or S_{ij}, require the inclusion of the leading elementary diagrams of exchange type.

We have carried out calculations for two homework potentials, Malfliet-Tjon and B1 Brink-Boeker potentials, and also for the central semi-realistic potential S3 by Afnan and Tang.

The relative importances of the elementary diagrams result to be quite similar for the various potentials.

The calculated one-body densities reveal strong correlation effects, particularly at small r, where up to 15% difference has been found between the correlated and the uncorrelated densities.

The FHNC-1 approximation is readily applicable to the case of state-dependent correlation operators, and therefore to the use of realistic nucleon-nucleon interactions.

Other interesting extensions of the FHNC-1 scheme are the treatment of $N \neq Z$ nuclei and the calculation of the one-body density matrix and of the momentum distribution. Work along these lines is in progress.

We are very grateful to E. Buendía, A.M. Lallena, S. Pieper and M. Viviani for providing us with unpublished VMC results. Part of the calculations have been performed using the CASPUR facility at NIC, Rome.

Appendix A

In this appendix we give the explicit expressions of the quantities which are used for the calculation of the energy expectation value, as shown in sect. 2.

The subindices have the following meaning: *d* means dynamical and indicates a point reached only by dynamical correlations, *e* means exchange and indicates a point reached by two statistical correlation (*e*-bonds). Finally *c* means cyclic and a point labelled with *c* is reached only by one *e*-bond belonging to a cyclic statistical permutation.

The diagrams are classified in:

- *nodal*, *N*, if they are containing at least an internal point where every path, joining the external points 1 and 2, has to pass through (for example the diagrams 1a, 1b and 1e),

- *composite*, X, if they can be decomposed in terms of nodal diagrams (fig. 1c, 1f)
- *elementary*, E, all the other kinds of diagrams (fig. 1d).

In the following we shall indicate the coordinate r_i as i and the convolution over 3 with the symbol ($|$). The sums of the nodal diagrams are

$$N_{dd}(1,2) = (X_{dd}(1,3)\xi_d(3) + X_{de}(1,3)\xi_e(3) | N_{dd}(3,2) + X_{dd}(3,2)) + (X_{dd}(1,3)\xi_e(3) | N_{de}(2,3) + X_{de}(2,3)), \quad (A.1)$$

$$N_{de}(1,2) = (X_{dd}(1,3)\xi_d(3) + X_{de}(1,3)\xi_e(3) | N_{de}(3,2) + X_{de}(3,2)), + (X_{dd}(1,3)\xi_e(3) | N_{ee}(2,3) + X_{ee}(2,3)), \quad (A.2)$$

$$N_{ee}(1,2) = (X_{ed}(1,3)\xi_d(3) + X_{ee}(1,3)\xi_e(3) | N_{de}(3,2) + X_{de}(3,2)) + (X_{ed}(1,3)\xi_e(3) | N_{ee}(2,3) + X_{ee}(2,3)). \quad (A.3)$$

To calculate the sum of the cyclic nodal diagrams, we used the following definitions:

$$N_{cc} = N_{cc}^{(x)} + N_{cc}^{(p)}, \quad (A.4)$$

with

$$N_{cc}^{(\alpha=x,p)} = N_{cc}^{\alpha x} + N_{cc}^{\alpha p}, \quad (A.5)$$

given by

$$N_{cc}^{xx}(1,2) = (X_{cc}(1,3)\xi_e(3) | X_{cc}(3,2) + N_{cc}^{xx}(3,2) + N_{cc}^{px}(3,2)), \quad (A.6)$$

$$N_{cc}^{xp}(1,2) = (X_{cc}(1,3)\xi_e(3) | -\rho_0(3,2) + N_{cc}^{xp}(3,2) + N_{cc}^{pp}(3,2)), \quad (A.7)$$

$$N_{cc}^{px}(1,2) = -(\rho_0(1,3)\xi_e(3) | X_{cc}(3,2) + N_{cc}^{xx}(3,2)) - (\rho_0(1,3)[\xi_e(3)-1] | N_{cc}^{px}(2,3)) \quad (A.8)$$

and

$$N_{cc}^{pp}(1,2) = -(\rho_0(1,3)\xi_e(3) | N_{cc}^{xp}(3,2)) - (\rho_0(1,3)[\xi_e(3)-1] | N_{cc}^{pp}(3,2) - \rho_o(3,2)), \quad (A.9)$$

with

$$N_{cc}^{xp}(1,2) = N_{cc}^{px}(2,1). \quad (A.10)$$

The $X_{\alpha\beta}$ functions have been defined as

$$X_{dd}(1,2) = g_{dd}(1,2) - N_{dd}(1,2) - 1, \quad (A.11)$$

$$X_{de}(1,2) = X_{ed}(2,1) = g_{dd}(1,2)[N_{de}(1,2) + E_{de}(1,2)] - N_{de}(1,2), \quad (A.12)$$

$$X_{ee}(1,2) = g_{dd}(1,2)\{N_{ee}(1,2) + E_{ee}(1,2) + [N_{de}(1,2) + E_{de}(1,2)]^2 - \nu[N_{cc}(1,2) - \rho_0(1,2) + E_{cc}(1,2)]^2\} \quad (A.13)$$

and

$$X_{cc}(1,2) = g_{dd}(1,2)[N_{cc}(1,2) - \rho_0(1,2) + E_{cc}(1,2)] - N_{cc}(1,2) + \rho_0(1,2), \quad (A.14)$$

where $E_{\alpha\beta}$ represent the sums of the $\alpha\beta$ elementary diagrams.

The distribution functions are now given by

$$g_{dd}(1,2) = f^2(1,2)\exp[N_{dd}(1,2) + E_{dd}(1,2)], \tag{A.15}$$

$$g_{de}(1,2) = g_{ed}(2,1) = X_{de}(1,2) + N_{de}(1,2), \tag{A.16}$$

$$g_{ee}^{dir}(1,2) = g_{dd}(1,2)\{N_{ee}(1,2) + E_{ee}^{dir}(1,2) + [N_{de}(1,2) + E_{de}(1,2)]^2\} + N_{ee}(1,2), \tag{A.17a}$$

$$g_{ee}^{exch}(1,2) = -\nu g_{dd}[N_{cc}(1,2) - \rho_0(1,2) + E_{cc}(1,2)]^2 + E_{ee}^{exch}(1,2) \tag{A.17b}$$

and

$$g_{cc}(1,2) = X_{cc}(1,2) + N_{cc}(1,2) - \rho_0(1,2). \tag{A.18}$$

The functions $U_{d,e}$ entering the vertex corrections $\xi_{d,e}$ are solutions of

$$\begin{aligned} U_d(r_1) = \int d^3r\, (&\{X_{dd}(r_1, r_2) - E_{dd}(r_1, r_2) - S_{dd}(r_1, r_2)[g_{dd}(r_1, r_2) - 1]\}\xi_d(r_2) \\ &+ \{X_{de}(r_1, r_2) - E_{de}(r_1, r_2) - S_{dd}(r_1, r_2)g_{de}(r_1, r_2) \\ &- S_{de}(r_1, r_2)[g_{dd}(r_1, r_2) - 1]\}\xi_e(r_2)), \end{aligned} \tag{A.19}$$

and

$$\begin{aligned} U_e(r_1) = \int d^3r\, (&\{X_{ed}(r_1, r_2) - E_{de}(r_1, r_2) \\ &- S_{dd}(r_1, r_2)g_{de}(r_1, r_2) - S_{ed}(r_1, r_2)[g_{dd}(r_1, r_2) - 1]\} \\ &+ \{X_{ee}(r_1, r_2) - E_{ee}(r_1, r_2) - S_{dd}(r_1, r_2)g_{ee}(r_1, r_2) \\ &- S_{ee}(r_1, r_2)[g_{dd}(r_1, r_2) - 1] - S_{ed}(r_1, r_2)g_{de}(r_1, r_2) \\ &- S_{de}(r_1, r_2)g_{ed}(r_1, r_2) + 2\nu S_{cc}(r_1, r_2)g_{cc}(r_1, r_2)\}\xi_e(r_2) \\ &- \nu\rho_0(r_1, r_2)[N_{cc}^{(p)}(r_1, r_2) - \rho_0(r_1, r_2)]), \end{aligned} \tag{A.20}$$

with

$$S_{mn} = \tfrac{1}{2}N_{mn} + E_{mn}. \tag{A.21}$$

Appendix B

In this appendix the expressions of the two-body densities defined in sect. 2 are given.

For the single-particle wave functions we use the representation

$$\phi_\alpha(1) \equiv \phi_{n,l,\mu}(r_1, s_1, t_1) = R_{n,l}(r_1)\, Y_{l,\mu}(\theta_1, \phi_1)\chi_s(1)\chi_t(1), \tag{B.1}$$

where $Y_{l,\mu}$ are the spherical harmonics, $R_{n,l}$ the radial wavefunctions and $\chi_{s,t}$ the spin and isospin spinors.

For the sake of simplicity, in the following we shall understand the subindex n of the radial wavefunction.

The $\rho_{T1}(r_1)$ defined in eq. (2.25) is a one-body density whose explicit expression is

$$\rho_{T1}(r_1)=\frac{\nu}{4\pi}\sum_{nl}(2l+1)\left(R_l(t_1)R_l''(r_1)+\frac{2}{r_1}R_l(r_1)R_l'(r_1)-R_l'(r_1)^2-2\frac{l(l+1)}{r_1^2}R_l^2(r_1)\right) \tag{B.2}$$

(in the present calculation $\nu=4$).

The uncorrelated two-body density defined in eq. (2.14) is given by

$$\rho_0(r_1, r_2)=\frac{2l+1}{4\pi}R_l(r_1)R_l(r_2)P_l(\cos\theta)\Xi(1,2)\,, \tag{B.3}$$

where P_l are the Legendre polynoms, θ the angle between the vectors r_1 and r_2, and

$$\Xi(i,j)=\sum_{ss't}\chi_s^\dagger(i)\chi_{s'}(j)\chi_t^\dagger(i)\chi_t(j)\,.$$

The density ρ_{T2} of eq. (2.8) is given by

$$\begin{aligned}\rho_{T2}(r_1, r_2)=&\frac{\nu}{(4\pi)^2}\sum_{nln'l'}(2l+1)(2l'+1)R_l(r_2)R_{l'}(r_2)\\&\times\left\{\left[R_l(r_1)\left(R_{l'}''(r_1)+\frac{2}{r_1}R_{l'}'(r_1)-\frac{l'(l'+1)}{r_1^2}R_{l'}(r_1)\right)\right.\right.\\&\left.\left.-R_l'(r_1)R_{l'}'(r_1)\right]P_lP_{l'}-\frac{\sin^2\theta}{r_1^2}R_l(r_1)R_{l'}(r_1)P_{l'}'\right\}\Xi(1,2)\,,\end{aligned} \tag{B.4}$$

where we have dropped the argument of the Legendre polynoms and of their derivatives.

The expression of the density ρ_{T3} of eq. (2.28) is

$$\rho_{T3}(r_1, r_2)=\frac{1}{4\pi}\sum_{nl}(2l+1)\left(R_l''(r_1)+\frac{2}{r_1}R_l'(r_1)-l(l-1)r^2R_l(r_1)\right)R_l(r_2)P_l\Xi(1,2)\,. \tag{B.5}$$

The density ρ_{T4} can be written as

$$\rho_{T4}(r_1, r_2)=\nu[\rho_{T6}(r_1, r_2)-\rho_0(r_1, r_2)\rho_{T5}(r_1, r_2)]\,, \tag{B.6}$$

with

$$\begin{aligned}\rho_{T5}(r_1, r_2)=&\frac{1}{4\pi}\sum_{nl}\left[\cos\theta\,R_l'(r_1)R_l'(r_2)P_l+\left(\frac{R_l(r_1)R_l'(r_2)}{r_1}+\frac{R_l(r_2)R_l'(r_1)}{r_2}\right)\right.\\&\left.\times\sin^2\theta\,P_l'+\frac{R_l(r_1)R_l(r_2)}{r_1r_2}[(1+\cos\theta)P_l'-\cos\theta\sin^2\theta\,P_l'']\right],\end{aligned} \tag{B.7}$$

and

$$\rho_{T6}(r_1, r_2) = \frac{1}{(4\pi)^2} \sum_{nln'l'} (2l+1)(2l'+1) R_l(r_2) R_{l'}(r_1)$$
$$\times \left[\sin^2\theta \left(\frac{R_l'(r_1) R_{l'}(r_2)}{r_2} P_l P_{l'}' + \frac{R_l(r_1) R_{l'}'(r_2)}{r_1} P_l' P_{l'} \right) \right.$$
$$\left. + \cos\theta \left(R_l(r_1)' R_{l'}'(r_2) P_l P_{l'} - \sin^2\theta \frac{R_l(r_1)' R_{l'}(r_2) P_l' P_{l'}'}{r_1 r_2} \right) \right]. \quad \text{(B.8)}$$

References

1) V.R. Pandharipande, Proc. Cargese summer School 1989, ed. J. Tran Tranh Van and J. Negele (Plenum, New York, 1990)
2) C.R. Chen, G.L. Payne, J.L. Friar and B.F. Gibson, Phys. Rev. **C33** (1986) 1740; A. Stadler, W. Glöckle and P.U. Sauer, Phys. Rev. **C44** (1991) 2319
3) J. Carlson, Phys. Rev. **C36** (1987) 2026
4) J. Carlson, V.R. Pandharipande and R. Schiavilla, *in*: Modern topics in electron-scattering, ed. B. Frois and I. Sick (World Scientific, Singapore, 1991)
5) M. Viviani, A. Kievsky and S. Rosati, Nuovo Cim. A (1992), in press
6) U. Helmbrecht and J.G. Zabolitzky, Nucl. Phys. **A442** (1985) 109
7) B.D. Day, Rev. Mod. Phys. **50** (1978) 495; B.D. Day and R.B. Wiringa, Phys. Rev. **C32** (1985) 1057; M. Baldo, I. Bombaci, S. Ferreira, G. Giansiracusa and U. Lombardo, Phys. Rev. **C43** (1991) 2605
8) R.B. Wiringa, V. Ficks and A. Fabrocini, Phys. Rev. **C38** (1988) 1010
9) O. Benhar, A. Fabrocini and S. Fantoni, *in*: Modern topics in electron-scattering, ed. B. Frois and I. Sock (World Scientific, Singapore, 1991)
10) V.R.P. Pandharipande and R.B. Wiringa, Rev. Mod. Phys. **51** (1979) 821
11) S. Rosati, *in*: From nuclei to particles, Proc. Int. School E. Fermi, course LXXIX, ed. A. Molinari (North-Holland, Amsterdam, 1982)
12) S.C. Pieper, R.B. Wiringa and V.R.P. Pandharipande, Phys. Rev. Lett. **64** (1990) 364; S. Pieper, *in*: Many-body theories, ed. Y. Avishai, vol. 2 (Plenum, New York, 1990)
13) R. Guardiola, A. Faessler, H. Müther and A. Polls, Nucl. Phys. **A371** (1981) 79
14) M.C. Boscá and R. Guardiola, Nucl. Phys. **A476** (1988) 471; R. Guardiola and M.C. Boscá Nucl. Phys. **A489** (1988) 45
15) S. Fantoni and S. Rosati, Nucl. Phys. **A328** (1979) 478
16) E. Krotscheck, W. Kohn and G.-X. Qian, Phys. Rev. **B32** (1985) 5693
17) E. Krotscheck, Nucl. Phys. **A465** (1987) 461
18) S. Fantoni and S. Rosati, Phys. Lett. **B84** (1979) 23
19) R.A. Malfliet and J.A. Tjon, Nucl. Phys. **A127** (1969) 161
20) D.M. Brink and E. Boeker, Nucl. Phys. **A91** (1967) 1
21) M.C. Boscá, E. Buendía, R. Guardiola, Phys. Lett. **B198** (1987) 312; Condensed matter theories, ed. J. Arponen, R. Bishop and M. Manninen, vol. 3 (Plenum, New York, 1987)
22) S. Pieper, private communication
23) I.R. Afnan and Y.C. Tang, Phys. Rev. **175** (1968) 1337
24) E. Buendía and A.M. Lallena, private communication
25) M. Viviani, private communication